
Chapter 10

High-frequency grounding

Leonid Grcev

10.1 Introduction

High-frequency and dynamic behaviour of grounding has been the subject of extensive theoretical and experimental research. Here, some representative work is listed containing useful material pertinent to the subject of this chapter. Pioneering but comprehensive work was conducted in the first half of the twentieth century, which is summarized by Sunde and others in well known reference books [1–3]. More recent work is summarized in the books in References 4 to 6. There is a lack of carefully documented experimental works in the literature, but noteworthy examples are found in References 7 to 10. The approaches on which some recent analytical work is based may be classified into the following groups:

- circuit theory [11–15]
- transmission line theory [16–21]
- electromagnetic field theory [22–28]
- hybrid approaches [29–31]

In spite of the large amount of work that has been devoted to this subject, there is still no consensus on how to apply present knowledge to the design of actual grounding for better high-frequency and dynamic performance. As a result, power-frequency ground impedance, which can easily be measured or calculated, is being used in most cases to predict grounding lightning performance [32].

10.2 Basic circuit concepts

High-frequency behaviour of grounding is of interest in lightning protection studies and is dependent on the high-frequency content of the lightning current pulses. Because the highest frequencies in a pulse spectrum are related to the fastest time variation, the lightning pulse usually has the highest frequency content during its rise, that is, during the first moments of the stroke. Grounding is usually designed for safety at industrial frequencies, principally because humans are more sensitive to 50/60 Hz

current than to current at high frequencies [33]. However, the performance of grounding systems might be much worse at high frequencies, which reduces the efficiency of the protection during the rise of the lightning current pulse, that is, during the first moments of the stroke. One reason for concern is the occurrence of high-intensity transient voltages that might endanger human safety and cause damage or malfunction in equipment during the first moments of the stroke. The highest voltage appears between the current feed point at the grounding system and a point at remote 'neutral' ground. This voltage, divided by the current, is referred to as ground impedance; lower values indicate better grounding system performance. Usually, the electric potential at the current feed point is used for the definition of the ground impedance instead of voltage. The low-frequency (50/60 Hz) ground resistance, which is practically equivalent to the direct current (d.c.) ground resistance, is a d.c. limit of the ground impedance.

Grounding may be considered by referring to a circuit with an ideal current source I with one terminal connected to the ground electrodes and the other terminal to the remote earth, theoretically at infinite distance (Figure 10.1). The influence of the connecting leads is ignored. The voltage between the current source terminals at d.c. is equivalent to the electric potential of the ground electrodes V with a reference point at remote earth. This enables definition of the ground resistance R as

$$R = \frac{V}{I} \quad (10.1)$$

Neglecting the influence of the current source connecting leads allows for extension of this concept to a general case of arbitrary time-varying excitation, because the path-dependent part of the voltage between current source terminals is ignored. Therefore, the voltage over the current source $i(t)$ is equivalent to the electric scalar potential at the current feed point $v(t)$, which allows for uniquely defined ground transient impedance $z(t)$:

$$z(t) = \frac{v(t)}{i(t)} \quad (10.2)$$

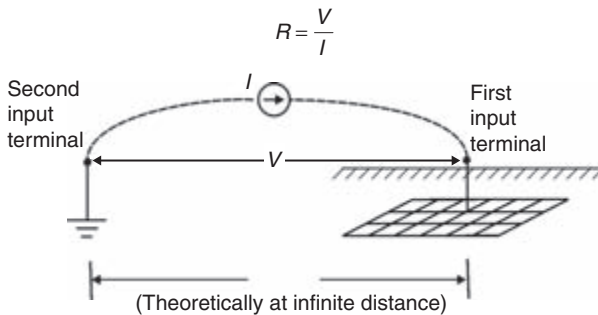


Figure 10.1 *Illustration of a theoretical circuit for evaluation of a d.c. ground resistance*

However, transient impedance is a characteristic that depends on the particular wave shape of the excitation $i(t)$.

Two practically equivalent approaches to excitation-independent ground impedance have been widely used. The first is the time-domain ground surge impedance $z_0(t)$, which is a ratio of the voltage response to a unit step current excitation. The second is the frequency-domain alternative to the surge impedance: ground harmonic impedance. As is well known, the harmonic impedance is a Fourier transform of the unit impulse response [34]. Because the unit impulse function has a constant spectrum, the harmonic impedance $\underline{Z}(\omega)$ may be evaluated simply by determining the voltage phasor $\underline{V}(\omega)$ as a response to a steady-state time harmonic current excitation $\underline{I}(\omega) = 1 - A$ in a frequency range up to the highest frequency of interest for the transient study:

$$\underline{Z}(\omega) = \frac{\underline{V}(\omega)}{\underline{I}(\omega)} \tag{10.3}$$

Here, $\omega = 2\pi f$, where f is frequency and the underscore denotes a complex variable. It is worth noting that the surge impedance can be determined from the harmonic impedance and vice versa [34]. For example, the surge impedance is given by [34]

$$z_0(t) = R + \frac{2}{\pi} \int_0^\infty \frac{X(\omega)}{\omega} \cos \omega t \, d\omega \tag{10.4}$$

where R is the d.c. ground resistance [see equation (10.1)] and $X(\omega)$ is the imaginary part of the harmonic impedance $\underline{Z}(\omega)$ [see equation (10.3)] (Figure 10.2).

Both surge and harmonic impedances depend solely on the geometry and the electromagnetic properties of the grounding system and the medium. As is well known, both can be used to determine the time response to an arbitrary excitation [34]. For example, voltage $v(t)$, as a response to an arbitrary current pulse $i(t)$, may be measured or taken from a simulated lightning current pulse, and is given by [25]

$$v(t) = \mathbf{F}^{-1} \{ \mathbf{F}[i(t)] \cdot \underline{Z}(\omega) \} \tag{10.5}$$

where \mathbf{F} and \mathbf{F}^{-1} denote Fourier and inverse Fourier transforms, respectively.

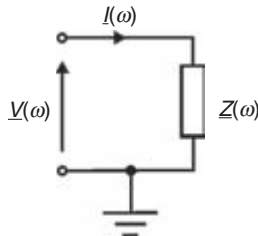


Figure 10.2 Harmonic ground impedance as a circuit element. The d.c. ground resistance is a limit for $\omega \rightarrow 0$.

A basic requirement for a frequency-domain analysis is that the system is linear, which makes this method unsuitable for modelling of non-linear phenomena. However, it is well suited for modelling important frequency-dependent phenomena.

When considering ground electrodes subjected to a lightning-related surge, analyses in the time and frequency domains are mutually related and the following statements apply.

- The initial surge state characterized by time-varying impedance is related to the high-frequency part of the harmonic impedance.
- The latter stationary condition characterized by fixed impedance is related to the low-frequency or d.c. resistance.

10.3 Basic field considerations

Circuit concepts in the previous section are the basis for engineering analysis, but field considerations are necessary for analysis of the limitations of the circuit concepts and for a better physical understanding of the grounding transient and high-frequency behaviour. A field approach is often also necessary to determine more precisely the ground impedances, particularly for cases of more complex grounding electrode arrangements, at high frequencies, and in more conductive earth. The usual simple model of earth is a homogeneous and isotropic half space with a plane interface with air, characterized by frequency-independent constitutive parameters: a fixed electrical conductivity σ on the order of ~ 0.0001 to 0.1 S m^{-1} , permittivity ε (with relative permittivity of ~ 10) and permeability identical to the permeability of air, $\mu = \mu_0$. Of these three constants, the conductivity exhibits by far the largest variations in its magnitude. In this analysis we will disregard the non-linear behaviour of the earth, which may arise as a result of high-intensity currents. However, as discussed in Section 10.8, many practically interesting consequences of frequency-dependent behaviour are not affected by non-linear behaviour.

It is important to distinguish between electromagnetic propagation in air and in the earth for the same frequency. The key quantity that gives a quantitative estimate related to the propagation effects is the TEM wave propagation constant $\underline{\Gamma}$, which in earth is given by [36]

$$\underline{\Gamma} = \alpha + j\beta = \sqrt{j\omega\mu_0(\sigma + j\omega\varepsilon)}$$

$$\alpha = \omega\sqrt{\mu_0\varepsilon} \left\{ \frac{1}{2} \left[\sqrt{1 + \left(\frac{\sigma}{\omega\varepsilon}\right)^2} - 1 \right] \right\}^{1/2}, \quad \beta = \omega\sqrt{\mu_0\varepsilon} \left\{ \frac{1}{2} \left[\sqrt{1 + \left(\frac{\sigma}{\omega\varepsilon}\right)^2} + 1 \right] \right\}^{1/2}$$
(10.6)

where α and β are attenuation and phase constants, respectively, and $j = \sqrt{-1}$.

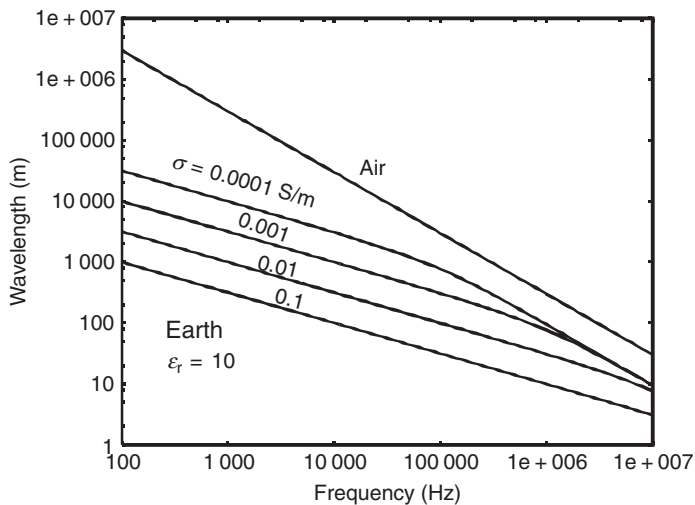


Figure 10.3 Wavelength in air and in earth with different conductivities

The parameters that are important to consider are λ (wavelength), v (velocity of propagation) and δ (skin depth):

$$\lambda = \frac{2\pi}{\beta}, \quad v = \frac{\omega}{\beta}, \quad \delta = \frac{1}{\alpha} \tag{10.7}$$

Figures 10.3 to 10.5 illustrate the strong dependence of λ , v and δ on the conductivity of the earth.

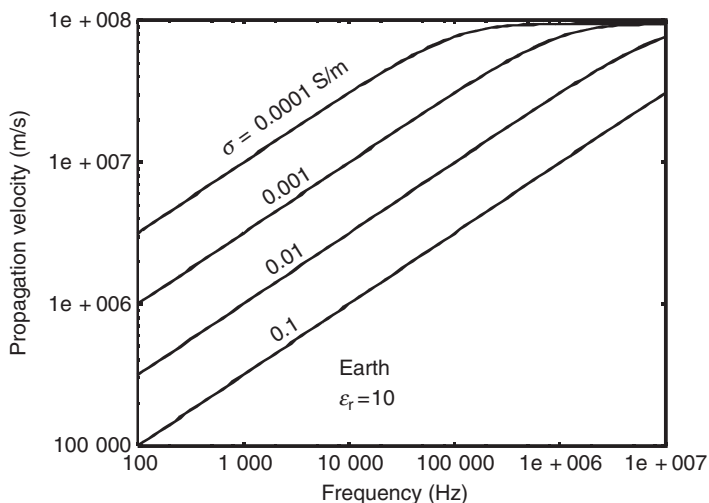


Figure 10.4 TEM wave propagation velocity in earth with different conductivities

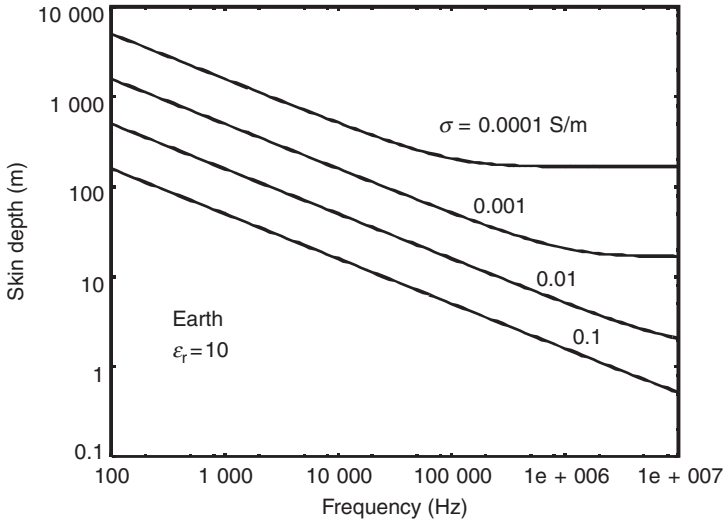


Figure 10.5 TEM wave skin depth in earth with different conductivities

Wavelength λ is smaller in earth than in the air, even for several orders of magnitude in more conductive soil and at lower frequencies (Figure 10.3). An important parameter related to wavelength is the electrical dimension of the system, which is a coefficient equal to the ratio of the physical dimension L and the wavelength λ . If the system’s electrical dimensions are much smaller than unity, then the electromagnetic waves do not experience significant change along such distances, and propagation effects can be neglected. In such a case, a quasi-static approximation can be applied for analysis. However, it is important to note that a system might have considerably larger electrical dimensions for the same frequency in earth than in air due to the smaller wavelengths there. As a result, the quasi-static approximation might be applicable in air but not in earth for the same buried system and frequency.

The velocity of propagation v [see equation (10.7)] is much smaller in earth than in air, particularly at low frequencies and for more conductive soil. It approaches the velocity of light at higher frequencies and in less conductive soil (Figure 10.4).

Figure 10.5 illustrates the skin depth δ [see equation (10.7)], that is, the distance the wave must travel in earth to reduce its value to 36.8 per cent of the value at the earth’s surface. Figure 10.5 illustrates the field tendency to localize near the source at higher frequencies.

The performance of grounding systems is determined by the rate of energy dissipation and storage in the soil. Based on Poynting’s theorem, terms of the mean values of power dissipated and stored in a volume V of soil can be evaluated [35] as follows:

$$\int_V \sigma |\vec{E}|^2 dV - \text{dissipated power (related to circuit resistive behaviour)}$$

$$\frac{1}{2} \int_V \epsilon |\vec{E}|^2 dV - \text{power stored in the electric field (related to circuit capacitive behaviour)}$$

$$\frac{1}{2} \int_V \mu_0 |\vec{H}|^2 dV - \text{power stored in the magnetic field (related to circuit inductive behaviour)}$$

Here, \vec{E} and \vec{H} are electric and magnetic field vector phasors, respectively.

The results in Figures 10.4 and 10.5 show that the volumes V available for dissipation and power storage are different at high and low frequencies, and also in the initial surge state and the latter stationary condition. A smaller V at high frequencies and in the surge state results in higher intensities of fields, current and potential near the feed point.

10.4 Frequency-dependent characteristics of the soil

In spite of the wide use of the frequency-independent model, it is well known, however, that in real earth the constitutive parameters σ and ϵ can be functions of frequency, with rather large variations in their values [36,37]. Tesche [38] recently studied the sensitivity of a calculated transient response to variations in these parameters. As discussed in Reference 36, the complex permittivity $\underline{\epsilon}$ and the complex conductivity $\underline{\sigma}$ may be assumed as

$$\underline{\sigma} = \sigma' - j\sigma'', \quad \underline{\epsilon} = \epsilon' - j\epsilon'' \tag{10.8}$$

Using real and imaginary parts of the complex permittivity and the complex conductivity (10.8) a real-valued, frequency-dependent effective permittivity and conductivity may be defined [38]:

$$\sigma_{\text{eff}}(\omega) = \omega\epsilon'' + \sigma', \quad \epsilon_{\text{eff}}(\omega) = \epsilon' - \frac{\sigma''}{\omega} \tag{10.9}$$

As an example, Figure 10.6 illustrates the measured frequency dependence of the effective relative permittivity and the effective conductivity of sandy soil with different water contents.

Tesche [38] has shown that Messier’s empirical model [40] for fitting the parameters for ϵ_{eff} and σ_{eff} given by the expressions

$$\epsilon_{\text{eff}}(\omega) = \epsilon_\infty + \sqrt{\frac{2\sigma\epsilon_\infty}{\omega}} \tag{10.10}$$

and

$$\sigma_{\text{eff}}(\omega) = \sigma + \sqrt{2\sigma\epsilon_\infty\omega} \tag{10.11}$$

can be rather accurate. Moreover, these expressions can be shown to provide causal results for computed responses, and hence they obey the Kramer–Kronig

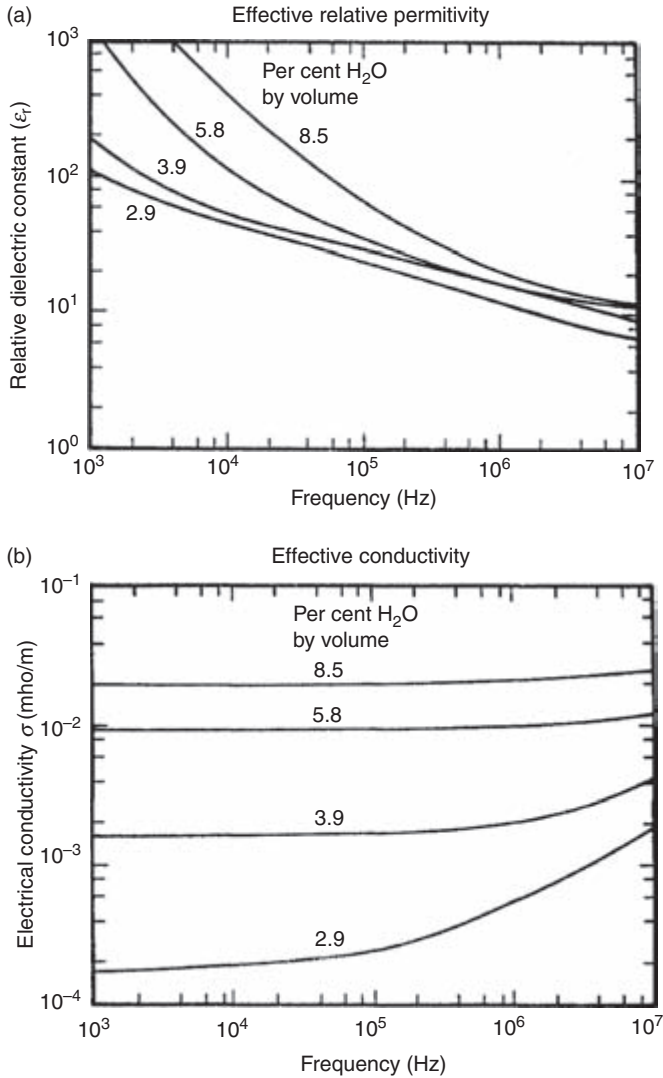


Figure 10.6 Plots of the measured relative effective permittivity (a) and the effective conductivity (b) of sandy soil with different water contents (by volume) (from Reference 39)

relationships [35]. This model for lossy earth depends only on two parameters: high-frequency permittivity ϵ_∞ and d.c. conductivity σ (together, of course, with the frequency).

For practical application of the above model, the measured data necessary for its implementation are rarely available. However, this phenomenon improves grounding system performance, so ignoring it always gives conservative results.

10.5 Grounding modelling for high frequencies

Vertical ground rods are one of the most simple and most commonly used means for earth termination of electrical and lightning protection systems [6] (Figure 10.7a). Their behaviour at 50 or 60 Hz is well understood using a simplified analysis based on static approximation [41]. By the traditional engineering approach at low frequencies, ground impedance of a single vertical rod is represented by a single resistor (Figure 10.7b), and at high frequencies by a lumped RLC circuit [3] (Figure 10.7c).

The classical expressions of lumped ground resistance R , inductance L , and capacitance C for a vertical rod are given by [1]

$$R = \frac{\rho}{2\pi\ell} A_1; \quad L = \frac{\mu_0\ell}{2\pi} A_1; \quad C = \frac{2\pi\epsilon\ell}{A_1} \tag{10.12}$$

$$A_1 = \ln \frac{4\ell}{a} - 1, \quad (\ell \gg a)$$

where ℓ and a are the length and radius of the rod, respectively (Figure 10.7a).

The parameters of the RLC circuit [see equation (10.12)] may be simply used to approximate the per unit length parameters of a distributed-parameter circuit [1] (Figure 10.7d):

$$R' = 1/G' = R\ell \text{ (}\Omega\text{ m)}; \quad L' = L/\ell \text{ (H m}^{-1}\text{)}; \quad C' = C/\ell \text{ (F m}^{-1}\text{)} \tag{10.13}$$

The transmission line may be considered to be open at the lower end, and the input impedance (equivalent to the harmonic ground impedance) is given by [1]

$$\underline{Z}(\omega) = \underline{Z}_0 \coth \underline{\gamma}\ell \tag{10.14}$$

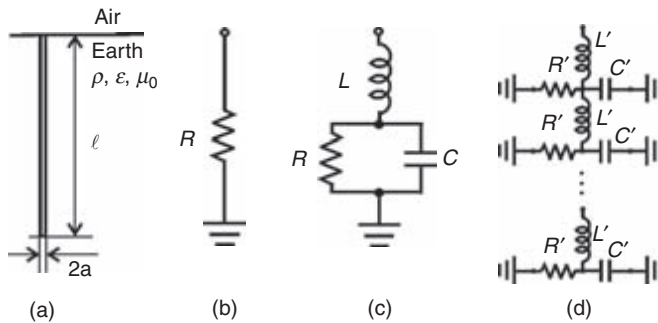


Figure 10.7 Low-current models of a vertical ground rod: (a) physical situation, (b) low-frequency equivalent circuit, (c) high-frequency lumped RLC circuit, (d) high-frequency distributed parameters circuit

Here $\underline{\gamma}$ and \underline{Z}_0 are the propagation constant and characteristic impedance, respectively [1]:

$$\underline{\gamma} = \sqrt{j\omega L'(G' + j\omega C')}; \quad \underline{Z}_0 = \sqrt{j\omega L'/(G' + j\omega C')} \quad (10.15)$$

Equations (10.12), (10.13) and (10.15) may be combined for the vertical rod:

$$\underline{\gamma} = \sqrt{j\omega\mu_0(\sigma + j\omega\varepsilon)}; \quad \underline{Z}_0 = \frac{A_1}{2\pi} \sqrt{\frac{j\omega\mu_0\rho}{(1 + j\omega\varepsilon\rho)}} \quad (10.16)$$

The logarithmic term A_1 [see equation (10.12)] involving ℓ cancels in the expression for $\underline{\gamma}$ [see equation (10.16)], but not for the case of \underline{Z}_0 . However, because the variation with ℓ is logarithmic, the results are not critically dependent on ℓ . The above per unit parameters are based on the TEM mode of propagation approximation. In a theoretical analysis, Roubertou and colleagues [22] have discussed the improper use of transmission line theory for the vertical rod and developed an approach based on electromagnetic theory. Figure 10.8 shows a comparison between computed impedances of two ground rods (the first one 3 m and the second one 30 m long) in earth with resistivity 100 Ω m and relative permittivity 10 by the three modelling approaches, based on lumped *RLC* circuit, transmission line and electromagnetic theory.

The impedance computed by the *RLC* model is in agreement with the other methods for rod lengths less than approximately one-tenth of the wavelength, which is in agreement with the conclusions of Reference 27. The model with the distributed-parameter circuit ('2' in Figure 10.8) follows the electromagnetic model ('3' in Figure 10.8), but it still significantly overestimates the values at higher frequencies. Better agreement between results is achieved for small rods in very resistive soil.

Similarly, the approximate modelling procedure for horizontal wires is based on classical lumped ground resistance R , inductance L and capacitance C formulae [1]:

$$R = \frac{\rho}{\pi\ell} A_2; \quad L = \frac{\mu_0\ell}{2\pi} A_2; \quad C = \frac{\pi\varepsilon\ell}{A_2} \quad (10.17)$$

$$A_2 = \ln \frac{2\ell}{\sqrt{2ad}} - 1, \quad (\ell \gg a, \quad d \ll \ell)$$

where d is the depth of burial.

Equations (10.12), (10.15) and (10.17) may be combined for the horizontal wire

$$\underline{\gamma} = \sqrt{j\omega\mu_0(1/\rho + j\omega\varepsilon)/2}; \quad \underline{Z}_0 = \frac{A_2}{\pi} \sqrt{\frac{j\omega\mu_0}{2(\sigma + j\omega\varepsilon)}} \quad (10.18)$$

The more accurate transmission line approach is based on Sunde's formulae for per unit length longitudinal impedance \underline{Z}' and transversal admittance \underline{Y}' [1]:

$$\underline{Z}'(\underline{\gamma}) \approx \frac{j\omega\mu_0}{2\pi} \ln \frac{1.85}{a\sqrt{\underline{\gamma}^2 + \underline{\Gamma}^2}}; \quad \underline{Y}'(\underline{\gamma}) \approx \pi(\sigma + j\omega\varepsilon) \left(\ln \frac{1.12}{\underline{\gamma}\sqrt{2ah}} \right)^{-1} \quad (10.19)$$

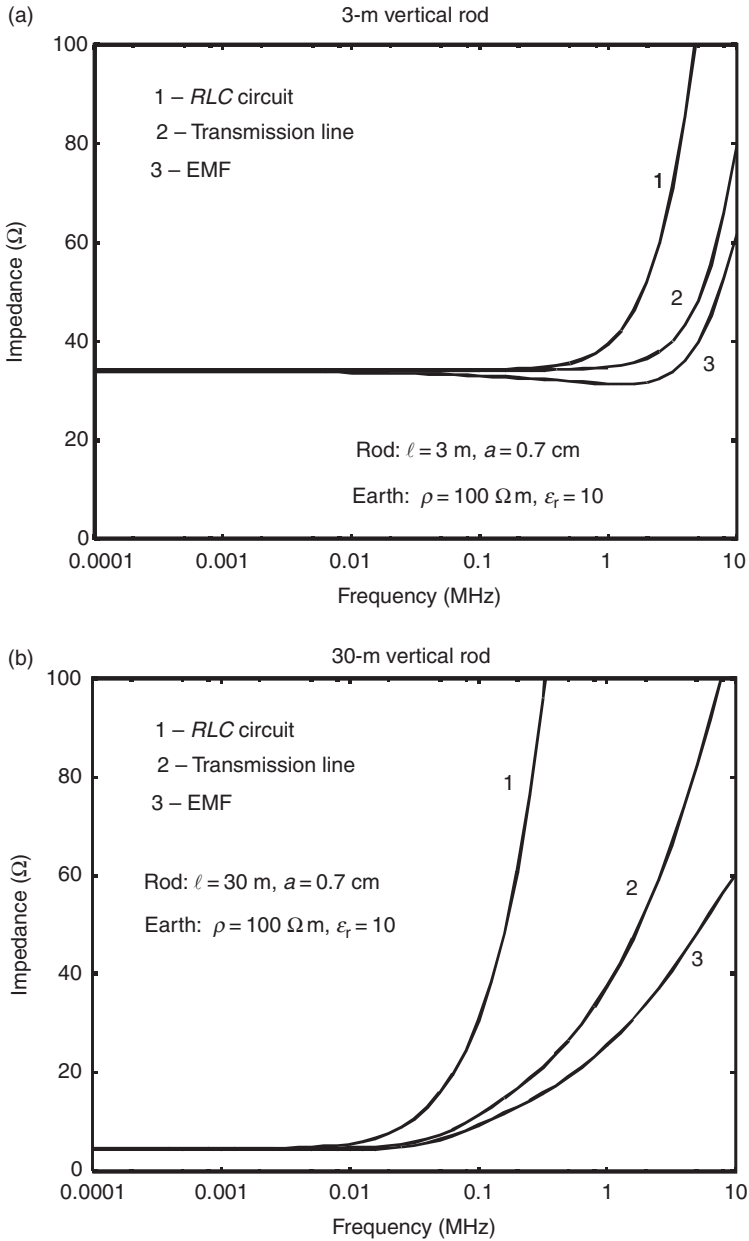


Figure 10.8 Comparison of results for harmonic ground impedance of vertical rods for (1) a lumped RLC equivalent circuit [equation (10.12)], (2) transmission line theory [equation (10.16)], (3) an electromagnetic field approach [22] in (a) a 3-m vertical rod and (b) a 30-m vertical rod

Solution of the transcendent equation

$$\gamma = \sqrt{Z'(\gamma) \cdot Y'(\gamma)} \quad (10.20)$$

yields a value for the propagation constant γ , which with substitution in equation (10.19) evaluates the characteristic impedance as

$$Z_0 = \sqrt{Z'(\gamma)/Y'(\gamma)} \quad (10.21)$$

and subsequently the ground impedance [see equation (10.14)].

The method in [25,26] is developed similarly to the previously developed method in [22]. Figure 10.9 presents a comparison of the results from the three modelling approaches, the transmission line approach based on equation (10.18) and equations (10.19) to (10.21) and the electromagnetic field approach [26]. Results for short wires (10 m) at high frequencies are in good agreement for the case in Figure 10.9a, but the approach based on equations (10.19) to (10.21) is not applicable for frequencies lower than 100 kHz. For longer wires (100 m) the model based on equation (10.18) ('1' in Figure 10.9) overestimates the values at higher frequencies, while the model based on equations (10.19) to (10.21) ('2' in Figure 10.9) follows the electromagnetic model ('3' in Figure 10.9).

Different modelling approaches have been developed for more complex grounding electrodes arrangements (mentioned in Section 10.1). There is no available systematically developed and reliable set of experimental data that would serve as a standard, so the electromagnetic model is used for the results in the rest of this chapter.

10.6 Frequency-dependent grounding behaviour

Figure 10.10 shows typical frequency dependence of the grounding harmonic impedance. The figure shows the ratio of the impedance modulus $|Z(\omega)|$ and the low-frequency ground resistance R . Two frequency ranges may be distinguished: the low-frequency range, where the impedance is nearly constant, that is, frequency independent, and the high-frequency range, where impedance is frequency dependent. Speaking in circuit terms, the high-frequency grounding behaviour may be categorized as inductive when $|Z(\omega)|/R > 1$, resistive when $|Z(\omega)|/R \approx 1$, or capacitive when $|Z(\omega)|/R < 1$. The important parameter in the case of inductive behaviour is the limiting frequency between the low-frequency and high-frequency ranges, the characteristic frequency F_c [44]. Figure 10.10 also illustrates the dominant influence of the earth's resistivity on the grounding frequency-dependent behaviour, because the same electrode behaves differently in earths with different resistivity.

Resistive and capacitive behaviour is advantageous because the high-frequency impedance is equal to or smaller than the low-frequency resistance to earth and consequently the grounding high-frequency performance is the same or better than at low frequencies. However, this is typical usually only for electrodes with smaller dimensions and in more resistive soils. More frequently the lengths of the electrodes and the earths' characteristics are such that the grounding exhibits inductive behaviour and

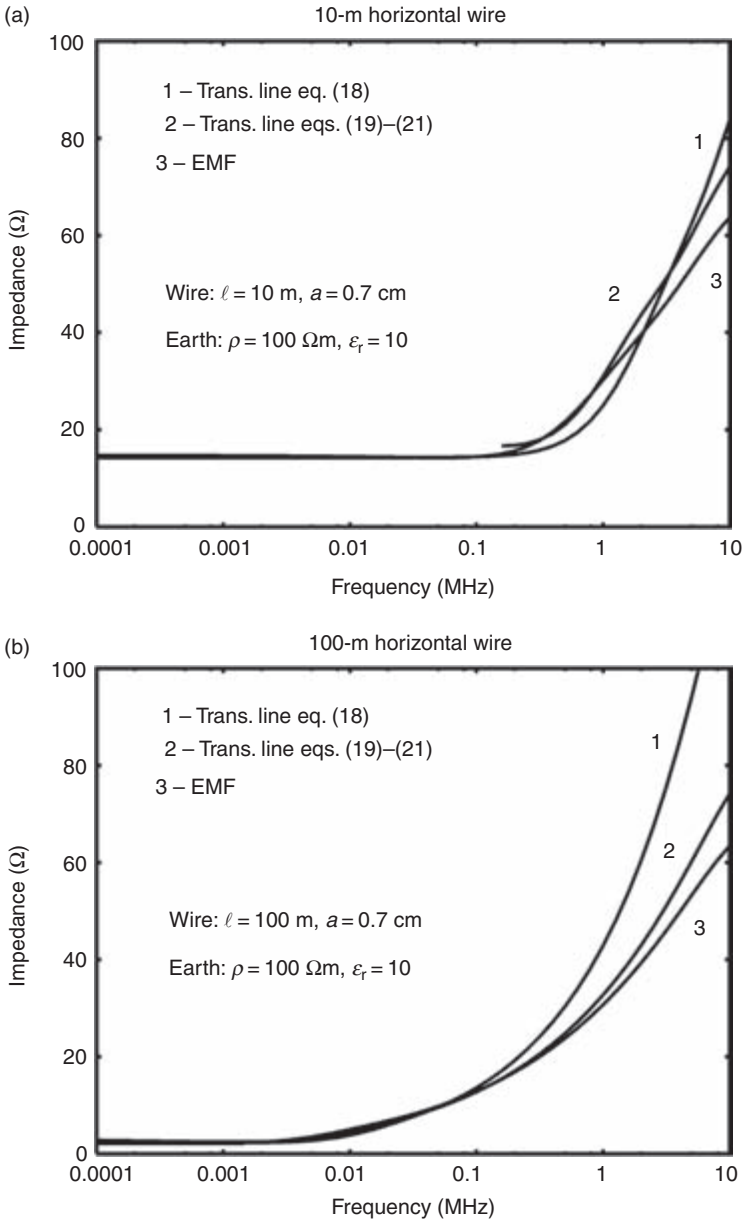


Figure 10.9 Comparison of results for harmonic ground impedance of horizontal wires for (1) transmission line equation (10.18), (2) transmission line equations (10.19) to (10.21), (3) the electromagnetic field approach [26] in (a) a 10-m horizontal wire and (b) a 100-m horizontal wire

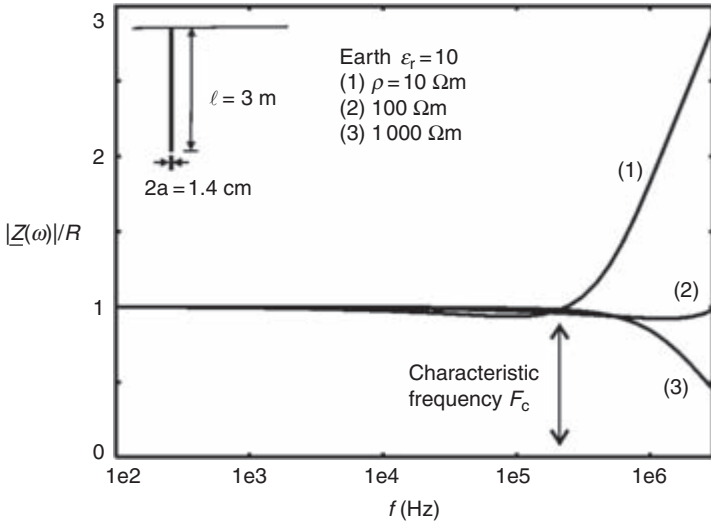


Figure 10.10 Typical frequency-dependent behaviour of the harmonic ground impedance: (1) Inductive behaviour; (2) resistive behaviour; (3) capacitive behaviour

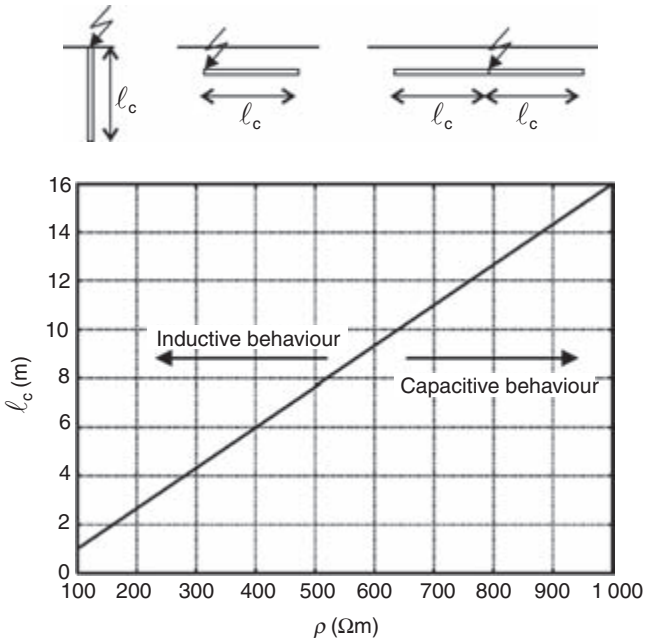


Figure 10.11 Regions of inductive and capacitive behaviour of grounding electrodes

consequently worse high-frequency performance. Figure 10.11 gives the regions of inductive and capacitive behaviour of vertical and horizontal rods depending on the earth's resistivity and the characteristic dimension ℓ_c , which is defined as a distance between the feed point and the most distant point of the grounding electrodes [43,44].

The first possibility for providing good high-frequency performance is to use smaller electrodes with capacitive or resistive behaviour. However, practically, this is seldom possible because longer electrodes are usually required to fulfil safety requirements at 50/60 Hz. Figure 10.12 illustrates typical high-frequency inductive ground impedance dependence on the grounding electrode length. Typically the characteristic frequency F_c is smaller for longer grounding electrodes with larger values of $\underline{Z}(\omega)$ in the high-frequency range and consequently with worse high-frequency performance. In addition F_c is also smaller in more conductive earth. For each characteristic frequency F_c there is a limiting length ℓ_R for low-frequency resistive behaviour, which is also referred to as the harmonic effective length (Figure 10.12).

One relation that determines such harmonic effective length ℓ_R as a function of the earth's resistivity ρ and the characteristic frequency F_c is [43,44]

$$\ell_R = 0.6(\rho/F_c)^{0.43} \tag{10.22}$$

Equation (10.22) is also illustrated in Figure 10.13.

It can be seen from Figure 10.12 that for frequencies higher than F_c , which corresponds to the harmonic effective length ℓ_R , all electrodes longer than ℓ_R exhibit nearly the same behaviour. This means that above F_c only the length ℓ_R of the electrode, measured from the feed point, effectively dissipates current into earth, regardless of how much longer the electrode is.

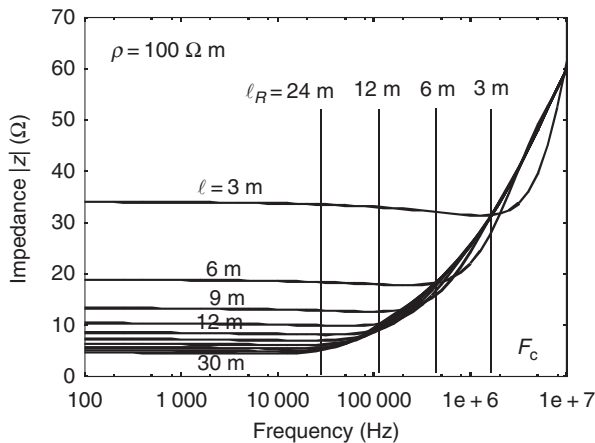


Figure 10.12 Harmonic impedance frequency dependence of horizontal wires in 100 Ω m earth

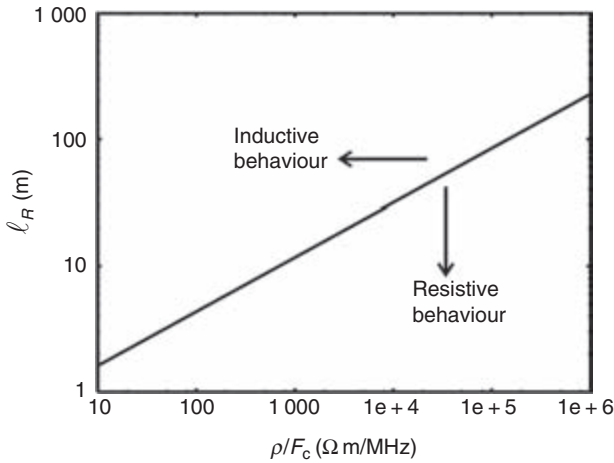


Figure 10.13 The limiting grounding electrode length for resistive behaviour

It has to be noted, however, that the practical importance of high-frequency behaviour in the case of pulse excitation depends on the frequency content of the excitation pulses. For example, if the frequency content of the lightning current pulses is lower than the characteristic frequency F_c , then the grounding behaviour will be resistive and not affected by the high-frequency inductive part of the impedance. As a first approximation, Gary [42] has suggested 100 kHz and 1 MHz frequency content for the first and subsequent strokes, respectively. This means that some electrodes that exhibit resistive behaviour for the first stroke might exhibit inductive behaviour for the subsequent stroke. This topic will be further discussed in Section 10.7.

The frequency-dependent analysis of more complex grounding electrode arrangements can also be based on the characteristic dimension, that is, the distance between the feed point and the most distant point of the arrangement. Figure 10.14 illustrates the influence of feed point location [28] on the high-frequency inductive behaviour of grid-like grounding electrode arrangements. It should be noted that for the corner feed point the characteristic dimension of the grounding grid is the length of the diagonal and is twice as large as for the centre feed point. As expected, the central feed point, that is, the smaller characteristic dimension, leads to higher characteristic frequency F_c , i.e. to better high-frequency performance. Having a central feed point rather than a corner one (in other words, twofold smaller characteristic dimension) broadens the low-frequency range with resistive behaviour by a factor of ten, i.e. from 1 kHz to nearly 10 kHz for soil with $\rho = 100 \Omega$ m and from 10 to 100 kHz for soil with $\rho = 1000 \Omega$ m. In addition, in the high-frequency range the impedance for the central feed point arrangement is two times smaller than that of the corner feed point.

The influence of grounding grid size on harmonic impedance is illustrated in Figure 10.15. Five square ground grids with 10 m to 10 m square mesh are chosen for computations, with dimensions ranging from 10 m \times 10 m to 120 m \times 120 m.

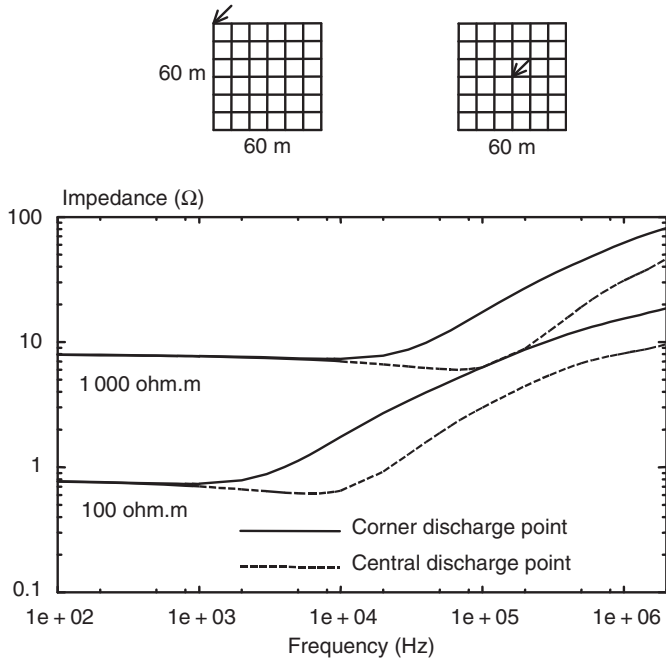


Figure 10.14 Influence of feed point location on harmonic impedance

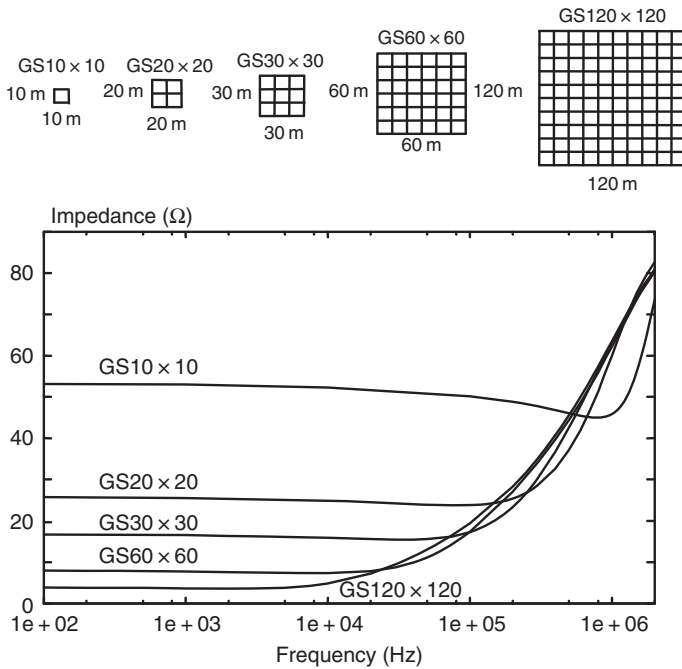


Figure 10.15 Influence of ground grid size on harmonic impedance

All grids are in soil with $\rho = 1\,000\ \Omega\ \text{m}$, $\epsilon_r = 9$ and with the feed point at the corner, so the characteristic dimension is always the length of the diagonal. Grounding grid characteristic dimension in Figure 10.15 has a similar influence as the single electrode in Figure 10.12. As for the single grounding wire, grounding grid size has a large influence on the low-frequency value of impedance to ground, but in the high-frequency range the behaviour of the different ground grids above a certain frequency becomes very similar. Clearly, the effective area of the grounding grids becomes smaller for higher frequencies.

The influence of grounding grid conductor separation on harmonic impedance is illustrated in Figure 10.16. Five square grounding grids with the same dimensions, $60\ \text{m} \times 60\ \text{m}$, with the number of meshes ranging from 4 to 124, are chosen for comparison. All grids are in soil with $\rho = 1\,000\ \Omega\ \text{m}$ and $\epsilon_r = 10$. The feed point is at the corner. As is well known, ground grid conductor separation has only a small influence on the low-frequency ground resistance, for which the dominant influence is the area of the grid. A similar conclusion is valid for the high-frequency behaviour of ground grids when conductor separation is reduced from 30 m to 6 m by introducing denser square meshes. A greater influence on the reduction of impedance in the high-frequency range (in other words, on an improvement in high-frequency performance) is achieved through a further reduction of conductor separation to 3 m near the feed point, that is, in the effective area.

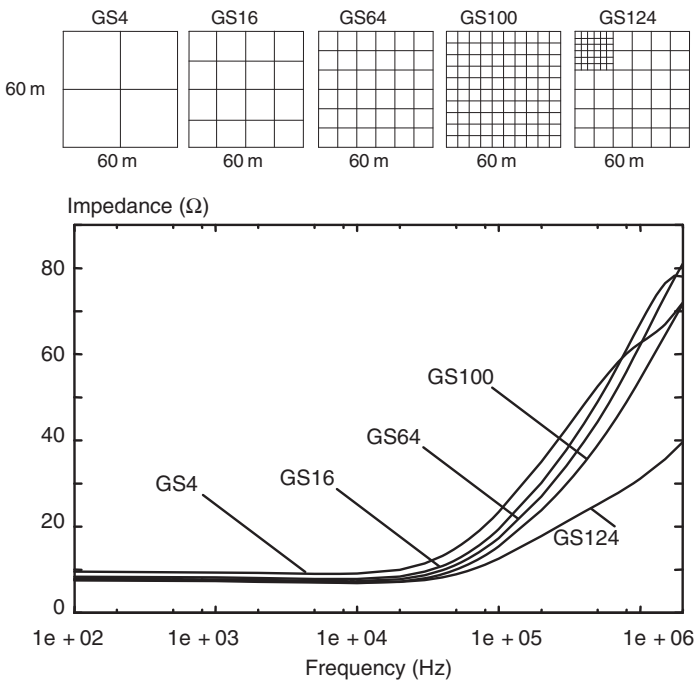


Figure 10.16 *Influence of conductor separation on harmonic impedance*

10.7 Frequency-dependent dynamic grounding behaviour

Here, we consider only the frequency-dependent aspects of dynamic behaviour. The non-linear behaviour of soil due to high currents is disregarded. However, in Section 10.8 the relation between frequency-dependent and non-linear dynamic behaviour will be discussed.

When harmonic impedance $Z(\omega)$ [see equation (10.3)] is determined, then the time function of the electric potential at the feed point $v(t)$ as a response to an injected lightning current pulse $i(t)$ can be evaluated [see equation (10.5)]. Several parameters are used to characterize dynamic behaviour of earth electrodes. One is transient impedance $z(t)$ [see equation (10.2)]. Usually, the impulse impedance Z is used, which is defined as the ratio between the peak values of $v(t)$ and $i(t)$:

$$Z = \frac{\max[v(t)]}{\max[i(t)]} = \frac{V_{\max}}{I_{\max}} \tag{10.23}$$

Another usual parameter is the impulse coefficient (efficiency), defined as the ratio between the impulse impedance and the resistance at low frequency, Z/R . It is worth noting that values of impulse coefficient larger than one are related to poorer transient performance.

The meaning of these parameters will be illustrated in an example. Consider a 12-m-long vertical rod constructed of copper with radius 0.7 cm in earth with a resistivity of $100 \Omega \text{ m}$ and relative permittivity of 10. Figure 10.17 shows the modulus of the harmonic impedance.

It can be seen that harmonic impedance is frequency independent and is equal to the low-frequency resistance to ground, $R = 10.3 \Omega$, up to the characteristic frequency, $F_c \approx 100 \text{ kHz}$. For higher frequencies, it exhibits inductive behaviour and its value becomes larger than R . The influence of such larger high-frequency values of $Z(\omega)$

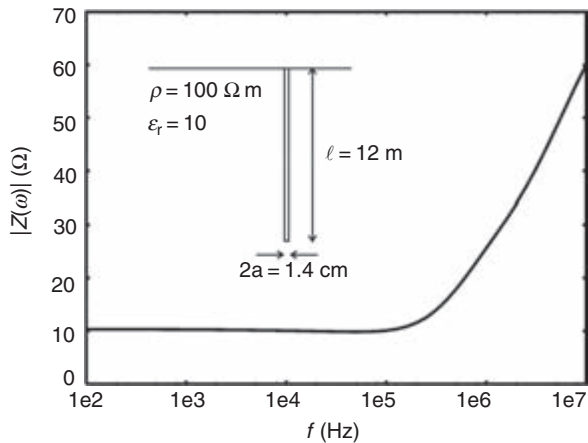


Figure 10.17 Modulus of the harmonic impedance to ground of a 12-m vertical rod

on the transient response depends on the frequency content of the excitation lightning current impulse.

Figure 10.18a shows the injected lightning current pulse typical for the first stroke $i(t)$, and the response to this excitation, the potential at the feeding point $v(t)$, and the transient impedance $z(t)$ [see equation (10.2)]. The procedure of determining the response $v(t)$ in equation (10.5) may be interpreted as passing the excitation $i(t)$ through a ‘filter’ with a frequency characteristic given by the harmonic impedance $Z(\omega)$ in Figure 10.17. The first stroke current pulse $i(t)$ (Figure 10.18a) has zero-to-peak time of about $8.4 \mu\text{s}$ and maximum steepness of $\sim 12 \text{ kA s}^{-1}$. Consequently, it does not have significant frequency content above the characteristic frequency of about $F_c \approx 100 \text{ kHz}$ (Figure 10.17), and is not affected by the high-frequency part of the ‘filter’. The response is mostly determined by the frequency-independent part, that is, the pure resistive part of the harmonic impedance, below F_c (Figure 10.17). Consequently, the response, that is, the voltage pulse

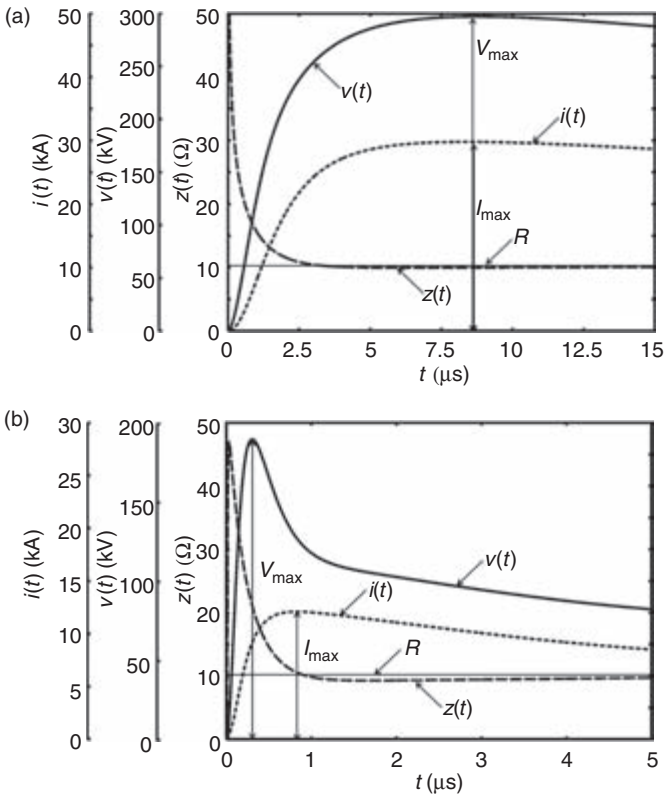


Figure 10.18 Lightning current pulse $i(t)$, transient voltage $v(t)$ and ground impedance of a 12-m ground rod: (a) response to a typical first stroke current pulse; (b) response to a typical subsequent stroke current pulse

waveshape, is not significantly modified in comparison to the current pulse waveshape and their maxima occur at the same time. Although the transient impedance $z(t)$ goes very quickly to some high value (larger than 50Ω), it quickly settles to the low-frequency resistance value ($R = 10.3 \Omega$) during the current rise. The transient impedance determines the duration of the transient period; here after about $3 \mu\text{s}$ the transient period is practically finished and a quasi-static analysis might subsequently be applied. The impulse coefficient is excellent, equal to one, that is, the impulse impedance is equal to the low-frequency resistance $Z = R$.

For the subsequent stroke current pulse injected in the same round rod the situation is different (Figure 10.18b). The subsequent stroke current pulse is more rapidly time-varying than the first stroke. It has a zero-to-peak time of $\sim 0.8 \mu\text{s}$ and maximum steepness of $\sim 40 \text{ kA s}^{-1}$. Consequently, it has significant frequency content above the characteristic frequency $F_c \approx 100 \text{ kHz}$ of the ‘filter’ (in Figure 10.17), and so the response is influenced by the inductive part of $Z(\omega)$. The ‘filter’ amplifies the high-frequency components of the pulse, which results in a large peak V_{max} of the transient voltage $v(t)$ during the rise of the current $i(t)$. Typically for inductive behaviour, the voltage pulse precedes the current pulse. This causes a larger value of the impulse impedance, $Z = 15.7 \Omega$, than the low-frequency resistance, $R = 10.3 \Omega$, and the impulse coefficient is equal to 1.5. The transient impedance $z(t)$, similar to the case of the first stroke (Figure 10.18a) rises very rapidly to a high value (of $\sim 47 \Omega$), but also quickly (in $\sim 1 \mu\text{s}$) settles to values near the low-frequency value, $R = 10.3 \Omega$, shortly after the occurrence of the peak of the current pulse.

The example in Figures 10.17 and 10.18 illustrates the fact that high-frequency inductive behaviour of grounding might result in large peaks of transient potential at the feed point in cases when the current pulses have enough high-frequency content to be influenced by high-frequency inductive behaviour. However, after a few microseconds, transient processes are practically finished and the transient impedance $z(t)$ settles to the value of the power-frequency resistance R .

Figure 10.19 shows the dependence of the impulse coefficient of vertical ground rods on their length and the earth’s resistance for the first and subsequent stroke current pulses [45].

It can be concluded that impulse performance is worse for longer rods in better conductive earth and for faster varying pulses, such as subsequent strokes. This effect is less important in less conductive soil and for not so quickly varying pulses, such as first strokes.

The dynamic effective length of a grounding rod is defined as the limiting length above which the impulse coefficient is larger than one. Values from Figure 10.19 are given in Table 10.1.

Figure 10.19 might be used for a first estimate of impulse efficiency and effective lengths of some other ground rod arrangements. Table 10.2 gives the percentage of the reduction of the impulse efficiency of the single vertical rod, given in Figure 10.19, for other multiple or horizontal grounding rod arrangements.

The use of multiple ground rod arrangements improves impulse efficiency. Horizontal rods are slightly less effective at power frequencies in comparison to vertical rods, but have better impulse efficiency.

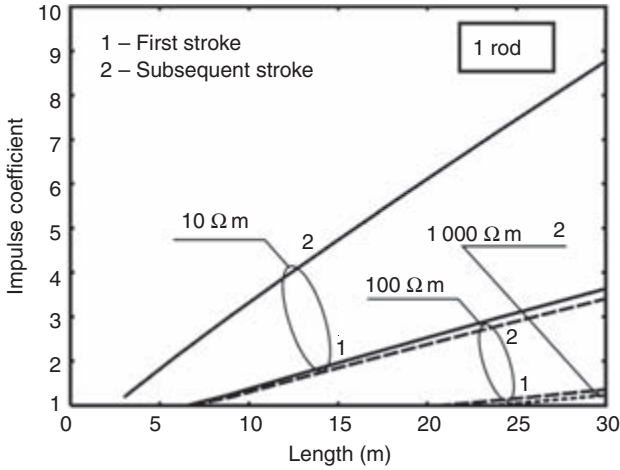


Figure 10.19 Impulse coefficient of a single vertical rod

Table 10.1 Dynamic effective lengths for the grounding rod in Figure 10.19

Earth's resistivity (Ω m)	Lightning stroke [45]	Vertical grounding rod dynamic effective length (m)
10	First	7.5
	Subsequent	3
100	First	22
	Subsequent	7.5
1 000	First	>30
	Subsequent	22

Table 10.2 Impulse coefficient and effective lengths of several ground rod arrangements

Ground rod arrangement						
Impulse coefficient (%)*	100	95	85	85	80	70
Effective length (%)*	100	105	118	118	125	143

*Percentage of values in Figure 10.19.

It should be emphasized that the impulse coefficient and the effective length that characterize possible worsening of the grounding performance during the lightning pulse in comparison with low-frequency performance are related only to the transient period, which may be very short (e.g. $3\ \mu\text{s}$ for the first stroke and $1\ \mu\text{s}$ for the subsequent stroke for the case in Figure 10.19).

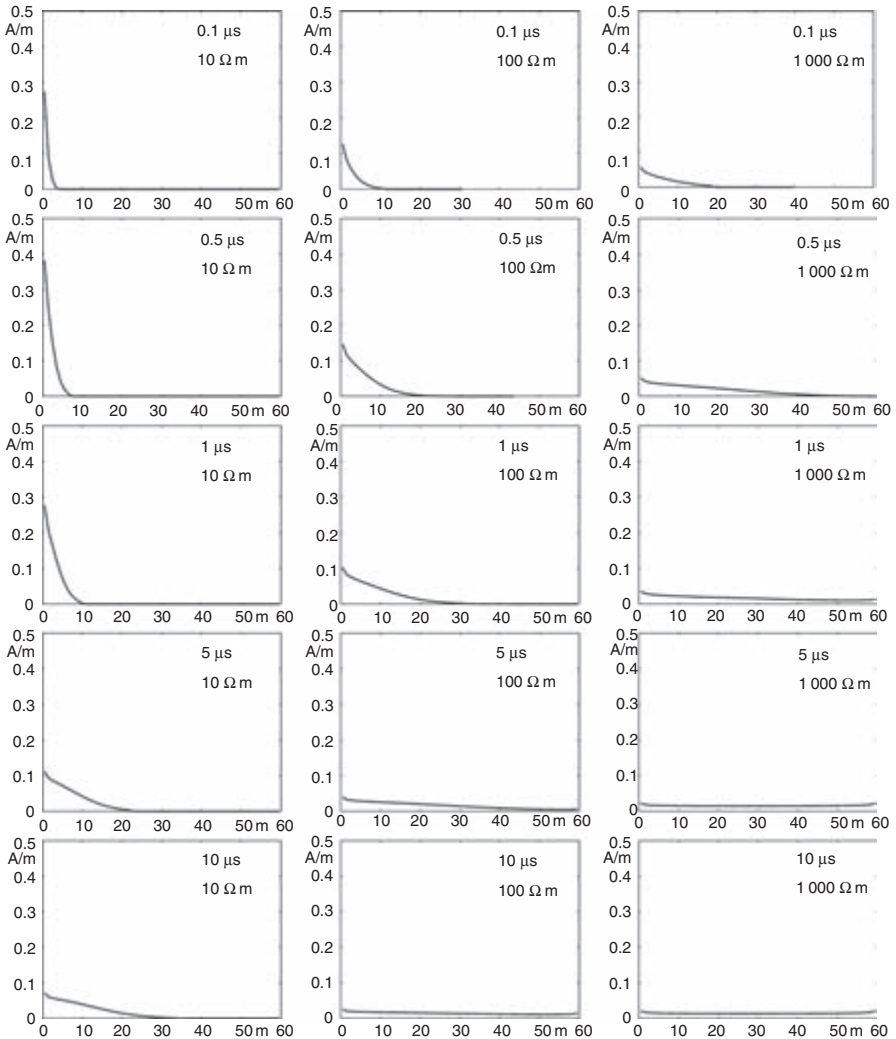


Figure 10.20 Temporal and spatial distribution of the leakage current along a 60-m-long horizontal wire as a response to an injected double-exponential ($T_1/T_2 = 1\ \mu\text{s}/50\ \mu\text{s}$) current pulse with a peak value 1 kA, at 0 m end in earths with resistivities of 10, 100 and 1 000 Ωm

10.8 Relation between frequency-dependent and non-linear grounding behaviour

When the electric field at the surface of the grounding electrode exceeds a value typically in the range 100 to 500 kV m⁻¹, electrical breakdown occurs in the surrounding earth [11,46]. This practically enlarges the dimensions of the grounding electrode and improves its performance.

The electric field at the surface of the grounding electrode is related to the leakage current:

$$\vec{J} = \sigma \cdot \vec{E} \quad (10.24)$$

Leakage current distribution characterizes the performance of the grounding electrodes because their main function is to dissipate the current to the earth. Figure 10.20 shows temporal and spatial distribution of the leakage current along a 60-m-long horizontal wire with radius $a = 0.7$ cm as a response to an injected double-exponential current pulse with a peak value 1 kA and zero-to-peak time $T_1 = 1$ μs and time-to-half $T_2 = 50$ μs, at the 0 m end in earths with resistivities of 10 Ω m (first column, Figure 10.20), 100 Ω m (second column, Figure 10.20) and 1 000 Ω m (third column, Figure 10.20). The velocity of electromagnetic field propagation is substantially smaller in less resistive earths, where a practically smaller part of the electrode is effective in dissipating current in the first moments of the stroke, resulting in larger values of the leakage current and electric field near the feed point. However, in more resistive earths, where non-linear phenomena are more likely to occur, due to the higher velocity of the electromagnetic field propagation, the transient period is smaller and a distribution equivalent to a d.c. (or 50/60 Hz) distribution of the leakage current (and electric field at the electrode surface) is spread over the whole length of the electrode very quickly after the beginning of the lightning pulse.

Table 10.3 gives the transient maximal and 50 Hz values of the current density and electric field for injected current with a peak value of 1 kA.

The critical electric field intensity for a soil breakdown (~ 300 kV m⁻¹) is reached in the case in Figure 10.20 even for 50 Hz in very resistive soil ($\rho = 1\,000$ Ω m).

Table 10.3 Maximal transient and 50 Hz values of the leakage current and electric field at the surface of the 60-m electrode at the feed point

Earth's resistivity (Ω m)		10	100	1 000
Maximal transient values	I' (kA m ⁻¹)	0.43	0.18	0.08
	E (kV m ⁻¹)	98	409	1 819
50 Hz values	I' (kA m ⁻¹)	0.016	0.016	0.016
	E (kV m ⁻¹)	3.6	36	364

Although the transient maximal values are larger, they last for a very short period of time (less than 1 μ s). On the other hand, soil ionization effects may last the large part of the pulse. However, since soil ionization usually improves the performance its neglect may be considered as an assumption on the 'safe' side. More accurate modelling that takes into account both soil ionization and frequency dependent effects is discussed in [48,49].

References

1. Sunde E.D. *Earth Conduction Effects in Transmission Systems*, 2nd edn. New York: Dover Publications, 1968.
2. Bewley L.V. *Traveling Waves on Transmission Systems*, 2nd edn. New York: Wiley, 1951.
3. Rudenberg R. *Electrical Shock Waves in Power Systems*. Cambridge: Harvard University Press, 1968.
4. Ryabkova E.Y. *Grounding in High Voltage Stations* (in Russian). Moscow: Energia, 1978.
5. Meliopoulos A.P. *Power System Grounding and Transients*. New York and Basel: Marcel Dekker, 1988.
6. Hasse P. and Wiesinger J. *Handbook for Lightning and Grounding*, 4th edn (in German). Munich: Pflaum, 1993.
7. Saint-Privat-d'Allier Research Group, 'Eight years of lightning experiments at Saint-Privat-d'Allier'. *Review Generale de l'Electricite (RGE)* 1982;**91**: 561–82.
8. Bourg S., Sacepe B. and Debu T. 'Deep earth electrodes in highly resistive ground: frequency behaviour'. *Proceedings of the 1995 IEEE International Symposium on Electromagnetic Compatibility*, 1995, pp. 584–89.
9. Stojkovic Z., Savic M.S., Nahman J.M., Salamon D. and Bukorovic B. 'Sensitivity analysis of experimentally determined grounding grid impulse characteristics'. *IEEE Transactions on Power Delivery* 1998;**13**(4):1136–42.
10. Sekioka S., Hayashida H., Hara T. and Ametani A. 'Measurements of grounding resistances for high impulse currents'. *IEE Proceedings – Generation, Transmission and Distribution* 1998;**145**(6):693–99.
11. Liew A.C. and Darveniza M. 'Dynamic model of impulse characteristics of concentrated earths'. *Proceedings of IEE* 1974;**121**(2):123–135.
12. Ramamoorthy M., Narayanan M.M.B., Parameswaran S. and Mukhedkar D. 'Transient performance of grounding grids'. *IEEE Transactions on Power Delivery* 1989;**PWRD-4**:2053–59.
13. Geri A. 'Behaviour of grounding systems excited by high impulse currents: the model and its validation'. *IEEE Transactions on Power Delivery* 1999;**14**(3):1008–17.
14. Otero A.F., Cidras J. and del Alamo J.L. 'Frequency-dependent grounding system calculation by means of a conventional nodal analysis technique'. *IEEE Transactions on Power Delivery* 1999;**14**(3):873–78.

15. Grcev L. and Popov M. 'On high-frequency circuit equivalents of a vertical ground rod'. *IEEE Transactions on Power Delivery* 2005;**20**(2):1598–1603.
16. Devgan S.S. and Whitehead E.R. 'Analytical models for distributed grounding systems'. *IEEE Transactions on Power Apparatus and Systems* 1973;**PAS-92**:1763–81.
17. Mazzetti C. and Veca G.M. 'Impulse behavior of grounded electrodes'. *IEEE Transactions on Power Apparatus and Systems* 1983;**PAS-102**:3148–56.
18. Velazquez R. and Mukhedkar D. 'Analytical modeling of grounding electrodes'. *IEEE Transactions on Power Apparatus and Systems* 1984;**103**:1314–22.
19. Menter F. and Grcev L. 'EMTP-based model for grounding system analysis'. *IEEE Transactions on Power Delivery* 1994;**9**:1838–49.
20. Liu Y., Zitnik M. and Thottappillil R. 'An improved transmission-line model of grounding system'. *IEEE Transactions on Electromagnetic Compatibility* 2001;**43**:348–55.
21. Liu Y., Theethayi N. and Thottappillil R. 'An engineering model for transient analysis of grounding system under lightning strikes: nonuniform transmission-line approach'. *IEEE Transactions on Power Delivery* 2005;**20**(2):722–30.
22. Roubertou D., Fontaine J., Plumey J.P. and Zeddani A. 'Harmonic input impedance of earth connections'. *Proceedings of the 1984 IEEE International Symposium on Electromagnetic Compatibility*, 1984, pp. 717–20.
23. Dawalibi F. 'Electromagnetic fields generated by overhead and buried short conductors, part I – single conductor'. *IEEE Transactions on Power Delivery* 1986;**PWRD-1**(4):105–11.
24. Dawalibi F. 'Electromagnetic fields generated by overhead and buried short conductors, part II – ground networks'. *IEEE Transactions on Power Delivery* 1986;**PWRD-1**(4):112–19.
25. Grcev L. and Dawalibi F. 'An electromagnetic model for transients in grounding system'. *IEEE Transactions on Power Delivery* 1990;**5**(4):1773–81.
26. Grcev L. 'Computer analysis of transient voltages in large grounding systems'. *IEEE Transactions on Power Delivery* 1996;**11**(2):815–23.
27. Olsen R. and Willis M.C. 'A comparison of exact and quasi-static methods for evaluating grounding systems at high frequencies'. *IEEE Transactions on Power Delivery* 1996;**11**:1071–81.
28. Grcev L. and Heimbach M. 'Frequency dependent and transient characteristics of substation grounding system'. *IEEE Transactions on Power Delivery* 1997;**12**(1):172–78.
29. Papalexopoulos A.D. and Meliopoulos A.P. 'Frequency dependent characteristics of grounding systems'. *IEEE Transactions on Power Delivery* 1987;**PWRD-2**:1073–81.
30. Heimbach M. and Grcev L. 'Grounding system analysis in transients programs applying electromagnetic field approach'. *IEEE Transactions on Power Delivery* 1997;**12**(1):186–93.
31. Visacro S. and Soares A. 'HEM: a model for simulation of lightning-related engineering problems'. *IEEE Transactions on Power Delivery* 2005;**20**(2):1206–208.

32. Chowdhuri P. *Electromagnetic Transients in Power Systems*. New York: Wiley, 1996.
33. IEEE Std. 80-2000, *IEEE Guide for Safety in AC Substation Grounding*. New York: IEEE, 2000.
34. Papoulis A. *The Fourier Integral and its Applications*. New York: McGraw-Hill, 1962.
35. Balanis C.A. *Advanced Engineering Electromagnetics*. New York: Wiley, 1989.
36. Ramo S., Whinnery J.R. and van Duzer T. *Fields and Waves in Communication Electronics*, 3rd edn. New York: Wiley, 1994.
37. Visacro S. and Portela C.M. 'Investigation of earthing system behavior on the incidence of atmospheric discharges at electrical systems'. *Proceedings of ICLP*, Interlaken, Switzerland, 1990, 3.8p.
38. Tesche F.M. 'On the modeling and representation of a lossy earth for transient electromagnetic field calculations'. Theoretical note 367, Kirtland AFB, NM, July 2002.
39. Mallon C. *et al.* 'Low-field electrical characteristics of soil'. Theoretical note 315, Kirtland AFB, NM, January 1981.
40. Messier M.A. *The Propagation of an Electromagnetic Impulse through Soil: Influence of Frequency Dependent Parameters*, MRC-N-415. Santa Barbara, CA: Mission Research Corporation, February 1980.
41. Tagg G.F. *Earth Resistances*. London: George Newnes Ltd, 1964.
42. Gary C. 'L'impédance de terre des conducteurs enterrés horizontalement'. Presented at the *International Conference on Lightning and Mountains*, Chamonix, France, 1994.
43. Grcev L. 'Improved earthing system design practices for reduction of transient voltages'. Presented at *CIGRÉ*, Session, Paris, France, 1998.
44. Grcev L. 'Improved design of transmission line grounding arrangements for better protection against effects of lightning'. Presented at the *International Symposium on Electromagnetic Compatibility (EMC'98 ROMA)*, Roma, Italy, 1998.
45. Rachidi F., Janischewskyj W., Hussein A.M., Nucci C.A., Guerrieri S., Kordi B. and Chang J.-S. 'Current and electromagnetic field associated with lightning – return strokes to tall towers'. *IEEE Transactions on Electromagnetic Compatibility* 2001;**43**:356–67.
46. Wang J., Liew A.C. and Darveniza M. 'Extension of dynamic model of impulse behavior of concentrated grounds at high currents'. *IEEE Transactions on Power Delivery* 2005;**20**(3):2160–65.
47. Grcev L. 'Impulse efficiency of ground electrodes'. *IEEE Transactions on Power Delivery* 2009;**24**(1):441–51.
48. Grcev L. 'Lightning surge characteristics of earthing electrodes'. Presented at the *29th International Conference on Lightning Protection (ICLP)*, Uppsala, Sweden, 2008.
49. Grcev L. 'Time- and frequency-dependent lightning surge characteristics of grounding electrodes'. *IEEE Transactions on Power Delivery*, in press.